

A&A manuscript no.
(will be inserted by hand later)

Your thesaurus codes are:
08(08.05.1; 08.05.2; 08.13.2; 08.18.1; 08.19.3; 08.23.3)

ASTRONOMY
AND
ASTROPHYSICS

The radiation driven winds of rotating B[e] supergiants

Inti Pelupessy¹, Henny J.G.L.M. Lamers^{1,2}, and Jorick S. Vink¹

¹ Astronomical Institute, University of Utrecht, Princetonplein 5, NL-3584 CC, Utrecht, The Netherlands.
f.i.pelupessy@phys.uu.nl; lamers@astro.uu.nl; j.s.vink@astro.uu.nl

² SRON Laboratory for Space Research, Sorbonnelaan 2, NL-3584 CA, Utrecht, The Netherlands

Received 9 February 2000 / Accepted ???

Abstract. We have formulated the momentum equation for sectorial line driven winds from rotating stars including: (a) the oblateness of the star, (b) gravity darkening (von Zeipel effect), (c) conservation of angular momentum, (d) line driving specified by the force multiplier parameters (k , α , δ), (e) finite disk correction factors for an oblate star with gravity darkening for both the continuum and the line driving. The equations are solved numerically. We calculated the distribution of the mass flux and the wind velocity from the pole to the equator for the winds of B[e]-supergiants. Rotation decreases the terminal velocity in the equatorial region but hardly affects the wind velocity from the poles; it enhances the mass flux from the poles while the mass flux from the equator remains nearly the same. These effects increase with increasing rotation rates.

We also calculated models with a bi-stability jump around 25 000 K, using force multipliers recently calculated with a Monte Carlo technique. In this case the mass flux increases drastically from the pole to the equator and the terminal velocity decreases drastically from pole to equator. This produces a density contrast in the wind $\rho(\text{equator})/\rho(\text{pole})$ of about a factor 10 independent of the rotation rate of the star. We suggest that the observed density contrast of a factor $\sim 10^2$ of the disks of B[e] stars may be reached by taking into account the wind compression due to the trajectories of the gas above the critical point towards the equatorial plane.

Key words: stars: early type – stars: emission line, Be – stars: B[e] – stars: mass loss – stars: rotation – supergiants – stars: winds, outflows

1. Introduction

In this paper we study the effects of rotation on the radiation driven winds of early-type supergiants. We will focus

on the explanation for the occurrence of disks around fast rotating B[e] supergiants.

B[e] supergiants, also designated sgB[e] stars (Lamers et al. 1998), are B type supergiants that exhibit forbidden emission lines in their optical spectra. The observations of hybrid spectra, i.e. spectra with *broad* UV P Cygni features and *narrow* emission lines and dust emission of B[e] supergiants in the Magellanic Clouds led to the proposal of a disk wind model by Zickgraf et al.(1985). This model postulates a dense disk of outflowing material in a fast line driven wind to explain the observed characteristics of the spectra of these stars (see Zickgraf 1992). The stellar wind at the equator is about ten times slower than that at the pole. Also, the wind at the equator is about a hundred times denser than at the pole. Additional evidence for a two-component outflow has been obtained from polarimetric measurements, e.g. by Zickgraf & Schulte-Ladbeck (1989).

The precise mechanism behind the formation of these disks is still a mystery (Cassinelli 1998). It is however clear that the origin of an axisymmetric wind structure such as a disk may well be connected to the fast rotation of a star. Two theories using rotation in a different way have been considered for the formation of these disk winds:

- (1) The Wind Compressed Disk (WCD) model of Bjorkman & Cassinelli (1993), that invokes the kinematics of the winds from rotating stars. The streamlines of the gas in the wind from both hemispheres of a rapidly rotating star cross in the equatorial plane. The concentration of the gas and the shock in the equatorial plane produce an outflowing equatorial disk, with a thickness on the order of a few degrees. Owocki & Cranmer (1994) have argued that the motion to the equatorial plane may be counteracted by the radiation force perpendicular from the plane due to lines. However, this “wind-inhibition effect” may not be effective in winds with a strong density gradient in the equatorial direction. We return to this in Sect. 7.

- (2) The rotationally induced bi-stability model (RIB) of Lamers & Pauldrach (1991) invokes an increase in the mass flux from the equator and a decrease in the equatorial wind velocity compared to the poles from the bi-stability jump. This jump in mass flux and in wind velocity is due

Send offprint requests to: H.J.G.L.M. Lamers

Correspondence to: Astronomical Institute, Princetonplein 5, NL-3584 CC, Utrecht, The Netherlands

to the temperature difference between the pole and the equator of a fast rotating B[e] supergiant with gravity darkening. The jump will occur for stars with effective temperatures between 20 000 and 30 000 K.

In reality, both effects, i.e. the wind compression and the rotation induced bi-stability, may be operating together and amplifying one another in the line driven winds of rapidly rotating early-B stars. (For a detailed explanation of both models, see Lamers & Cassinelli (1999) (hereafter *ISW*), Chapter 11.)

The theory of radiation driven winds for non-rotating stars was developed by Castor et al. (1975) (hereafter CAK) and predicts the mass loss rate and v_∞ for spherical winds. The influence of rotation on line driven winds was investigated by Friend & Abbott (1986). They found an increase in the mass-loss rate at the equator and a corresponding decrease in v_∞ , but these authors did not consider the effects of gravity darkening and the oblate shape of the star. Cranmer & Owocki (1994) described the finite disk correction factor in case of an oblate star.

In this paper we will modify the line driven wind theory, including these effects of oblateness and gravity darkening as well as the rotational terms in the equation of motion. This will then be applied to rapidly rotating B[e] supergiants to investigate whether these effects can explain the occurrence of disks. We will also apply recent bi-stability calculations to study the effect of the RIB-model to explain the occurrence of outflowing disks around rapidly rotating B[e] supergiants.

In Sect. 2 we describe the theoretical background of the radiation driven wind theory and the bi-stability effect. In Sect. 3 we derive the equations for the winds from oblate rotating stars with a temperature gradient between poles and equator due to gravity darkening. In Sect. 4 we describe the method for solving the equations and for calculating the winds from rotating stars. These calculations will be applied to B[e] supergiants in Sect. 5. In Sect. 6 we will investigate the effect of bi-stability on rotating stars and Sect. 7 concludes with a summary of this work and a discussion on the formation of disks of B[e] supergiants.

2. Theoretical context

The computation of the dynamics of line driven stellar winds is a complicated problem in radiation hydrodynamics. It involves the simultaneous solution of the equations of motion, the rate equations and the radiative transfer equations in order to calculate the radiative acceleration.

For hot luminous stars the line forces are the most important driving forces in the wind. CAK have shown that the line acceleration can be parameterized in terms of the optical depth parameter $t \sim \rho(dr/dv)$ as $g_{\text{line}} \sim kt^\alpha$, where k and α are parameters that depend on composition and temperature of the wind. In this expression k is a measure of the number of lines and α is a measure of the

distribution of the line strengths with $\alpha = 0$ or 1 for a pure mix of optically thin or thick lines respectively.

In this paper we adopt the CAK formalism and simplify the equations of motion by assuming a stationary, radial flow of a viscousless fluid. The possible influence of magnetic fields will be ignored. These simplifications are subject to the following restrictions (see e.g. Abbott 1980):

- The CAK theory treats the line acceleration in a simplified way in terms of the force multipliers, described above. Detailed calculations of the line driving, including millions of lines, show that the total line acceleration can be well described by this simple representation (Pauldrach et al. 1986).
- Both observations and calculations show that line driven stellar winds are not stationary. Even a wind in a stationary solution will develop shocks (see e.g. Lucy 1982). However, the time-averaged structure follows the stationary state quite well (see Owocki et al. 1988, and Feldmeier 1999). Therefore we will restrict ourselves to stationary models.
- A sectorial model will be adopted. This means that for every latitude a one dimensional problem will be solved. Wind compression as in the WCD model will thus be neglected, but the main effect of wind compression is expected to *redistribute* the mass loss and not to change the *total* mass that is lost from the rotating star.
- The absence of viscosity is a good approximation at the high density of line driven winds (see CAK).

The representation of the line force by a simple power law may seem to be a gross simplification of the underlying physics of myriad line absorption processes, but it can be shown to hold for a homogeneously distributed mix of optically thick and thin lines (Abbott 1982, Gayley 1995). Calculations of CAK and more recently in NLTE by Vink et al. (1999) of realistic model atmospheres, based on calculations of unified atmosphere/wind models with the ISA-WIND code (de Koter et al. 1997), confirm this to be generally true to good accuracy for the important part of the wind (from about the sonic point up to a few stellar radii). Therefore, the complex physics of ion populations can be ignored in the investigation of the various effects of rotation on the stellar wind.

However, there is one notable exception which is called the bi-stability jump. This refers to a jump in v_∞ around the temperature of 21000 K where v_∞/v_{esc} climbs from 1.3 (lower temperature) to 2.6 (higher temperature). This jump was observed by Lamers et al. (1995) in B supergiants. It is linked to a shift in ionization states of Fe in the lower part of the wind. The line driving in the lower part of the wind is dominated by iron. Below about $T_{\text{eff}} \simeq 25000$ K, Fe IV recombines to Fe III and since Fe III is a more efficient line driver than Fe IV, the wind structure changes dramatically (Vink et al. 1999).

The bi-stability jump may also occur in the temperature difference between the pole and the equator of a fast rotating star with gravity darkening. Therefore two sets of force multiplier parameters for the wind will be adopted to reflect the sudden change in ionization states (a high-temperature set for the pole and a low-temperature set for the equator).

3. The physics of rotation

Intuitively it is clear that rotation has an effect on the shape of a star and on the motion of the gas in the wind. An additional effect that the rotation of a star can have is the darkening of the equatorial regions of a star via the von Zeipel effect. These effects will modify the wind of a star considerably and we will incorporate them in the line driven wind theory for rotating stars.

3.1. The shape of a rotating star

The shape of a uniformly rotating star with all its mass concentrated in the core is determined by the equipotential surfaces of the potential in a rotating frame (Roche model):

$$\Phi(x, \theta, \phi) = \frac{1}{x} + \frac{1}{2}\omega^2 x^2 \sin^2(\theta) \quad (1)$$

where $x = r/R_{\text{eq}}$, θ is the co-latitude ($\theta = 0$ at the pole) and $\omega = v_{\text{rot,eq}}/v_{\text{crit}}$. Φ is of course independent of the longitude ϕ . Note that $1 + 0.5\omega^2 = R_{\text{eq}}/R_{\text{pole}}$. So the maximum oblateness is $R_{\text{eq}}/R_{\text{pole}} = 3/2$. The critical (break-up) velocity is defined in this paper as:

$$v_{\text{crit}}^2 = GM_{\star}^{\text{eff}}/R_{\text{eq}} \quad (2)$$

where M_{\star}^{eff} is the effective mass of the star,

$$M_{\star}^{\text{eff}} = M_{\star}(1 - \Gamma_e) \quad (3)$$

which is the reduced mass due to radiation pressure by electron scattering (see below).

The surface of a rotating star is implicitly given by Eq. 1. Solving this expression for $x(\theta)$ is equivalent to the solution of a 3rd degree polynomial, which results in

$$x(\theta) = 2 \frac{\sqrt{2 + \omega^2}}{\sqrt{3} \omega \sin \theta} \sin \left\{ \frac{1}{3} \arcsin \left(\frac{3\sqrt{3} \omega \sin \theta}{(2 + \omega^2)^{3/2}} \right) \right\} \quad (4)$$

Because of the difference in radius

$$\frac{R_{\text{eq}}}{R_{\text{pole}}} = 1 + 0.5\omega^2 \quad (5)$$

and the difference in rotational velocity between pole and equator, the radial escape velocity at the equatorial region is smaller than at the pole

$$v_{\text{esc}}^{\text{eq}} = \sqrt{\frac{1 - 0.5\omega^2}{1 + 0.5\omega^2}} v_{\text{esc}}^{\text{pole}} \quad (6)$$

We can then roughly estimate the effect of rotation on v_{∞} as this value has an almost linear dependence on v_{esc} (see later in §4).

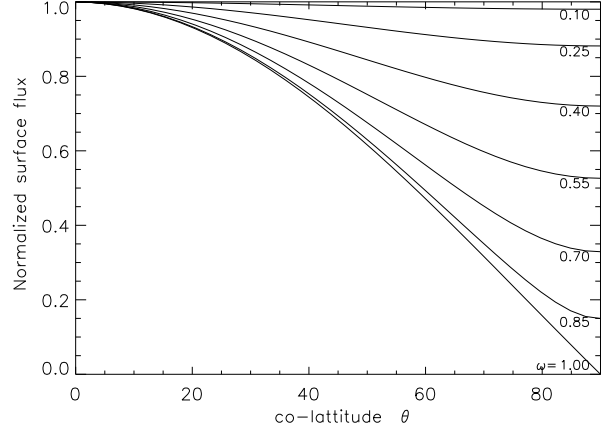


Fig. 1. Gravity darkening for different rotation rates ω as a function of co-latitude θ

3.2. Von Zeipel gravity darkening

The von Zeipel theorem (1924) for distorted stars states that the radiative flux from a point on the star is proportional to the local effective gravity:

$$F(\theta, \phi) = \sigma_B T_{\text{eff}}^4(\theta) \propto g_{\text{eff}}(\theta) \quad (7)$$

with σ_B the Boltzmann constant. As $g_{\text{eff}} = -\nabla\Phi$, we can write down the flux of a rotating star as a function of the co-latitude θ . This (lengthy) expression for the flux as a function of θ is plotted in Fig. 1 for a few different values of ω .

3.3. The equation of motion of a line driven wind of a rotating star

The rotation of the star can induce a θ component of the flow of the matter in the wind. In this study a possible θ component is neglected as was discussed in §2, but the motion in the longitudinal ϕ direction must still be taken into account.

In the absence of forces that can exert a torque on the wind, the equation of motion for v_{ϕ} is given by the conservation of angular momentum. Note however that there could be a torque from the line forces themselves, which is dependent on the velocity gradient of the gas. We assume that there are no external torques, so conservation of angular momentum gives:

$$v_{\phi}(r) = v_{\text{rot}}(R_{\star}) \frac{R_{\star}}{r} \quad (8)$$

The equation of motion for the radial direction becomes:

$$v \frac{dv}{dr} + \frac{GM_{\star}}{r^2} + \frac{1}{\rho} \frac{dp}{dr} - v_{\text{rot}}^2 \frac{R_{\star}^2}{r^3} - g_{\text{rad}} = 0 \quad (9)$$

where v is the radial velocity and M_{\star} is the stellar mass.

The conservation of mass for a non-spherical sectorial wind can be written as

$$4\pi r^2 \rho(\theta, r) v(\theta, r) = F_m(\theta) \quad (10)$$

where $F_m(\theta)$ is the "local mass loss rate," i.e. the total mass loss rate if the solution for this latitude were valid for a spherical star. The total mass loss rate from the star is

$$\dot{M} = \int_0^{\pi/2} F_m(\theta) \sin(\theta) d\theta \quad (11)$$

The equation of motion together with the conservation of mass governs the dynamics of the wind given the equation of state, $p = a^2 \rho$ (a is the isothermal sound speed), and the radiative acceleration g_{rad} . Using the conservation of mass, the pressure term can be rewritten as:

$$\frac{1}{\rho} \frac{dp}{dr} = \frac{1}{\rho} \frac{da^2}{dr} - \frac{2a^2}{r} - \frac{a^2}{v} \frac{dv}{dr} \quad (12)$$

As in the CAK-theory the temperature structure is specified a priori as a function of r . (The results depend only very weakly on the chosen temperature structure; see Pauldrach et al. 1986).

The radiative acceleration consists of two components. The continuum component due to the electron scattering, g_e , and a second component, g_L , due to line scattering and absorption processes. The continuum acceleration is given in terms of Γ_e :

$$g_e = \frac{\sigma_e F}{c} = \Gamma_e \frac{GM_\star}{r^2} \quad (13)$$

where σ_e is the electron opacity, L is the stellar luminosity and F is the radiation flux. The contributions by other continuum opacities are small. Nevertheless, they were included in the calculation of the force multipliers by Vink et al. (1999) used in our bi-stable wind models (Sect. 6).

For a homogeneous spherical star, Γ_e is given by¹:

$$\Gamma_e = \frac{\sigma_e L_\star}{4\pi GM_\star} \quad (14)$$

In the more general case of a non-homogeneous, non-spherical star the continuum acceleration can be defined as a correction to the 'classical' continuum acceleration of Eq. 14:

$$\Gamma'_e = D_c \frac{\sigma_e L_\star}{4\pi GM_\star} \quad (15)$$

where D_c is the continuum correction factor which is given by:

$$D_c = \frac{4\pi r^2}{L_\star} \oint_{\text{disk}} I(\theta, \phi) d\Omega \quad (16)$$

¹ Note: we define Γ_e as the ratio between the continuum force and gravity and not as the ratio between continuum force and the critical radiation force for a rotating star

The line acceleration $g_L(r, v, v')$ has a more complicated form, since it is a function of distance r as well as the velocity v and velocity gradient dv/dr . Combining the equation of motion (Eq. 9) with the rewritten pressure and continuum acceleration terms and multiplying by r^2 , one finds:

$$F_\theta(r, v, v') \equiv \left(1 - \frac{a^2}{v^2}\right) r^2 v \frac{dv}{dr} - v_{\text{rot}}^2 \frac{R_\star^2}{r} + GM_\star(1 - \Gamma'_e) - 2a^2 r - r^2 g_L = 0 \quad (17)$$

This equation is valid for each co-latitude θ . Following CAK, the critical point of this equation is found by imposing the singularity condition (where the subscript c indicates values at the critical point):

$$\left(\frac{\partial F_\theta}{\partial v}\right)_c = 0 \quad (18)$$

and the regularity condition:

$$\left(\frac{\partial F_\theta}{\partial r}\right)_c + \left(v' \frac{\partial F_\theta}{\partial v}\right)_c = 0 \quad (19)$$

Note that the critical point is not the sonic point r_s ($v(r_s) = a$) due to the fact that there is an additional dependence on v' in the line acceleration g_L (Abbott 1980; ISW Chapt 3.3).

3.4. The radiative line forces

The line forces are described within the framework of CAK in the Sobolev approximation. This means that the intrinsic line absorption profiles are considered to be infinitely sharp. Then the line force becomes a function of local properties of the wind only. The acceleration due to an ensemble of lines is given by the summation of the contributions of all individual lines with rest frequencies ν_l . g_L is given by (Castor 1974):

$$g_L = \sum_l \frac{\kappa_l}{c} \oint I_{\nu_l} \frac{1 - e^{-\tau_{\nu_l}}}{\tau_{\nu_l}} \mu d\Omega \quad (20)$$

where κ_l is the absorption coefficient per gram for the l th line, $\mu = \cos \theta$, I_{ν_l} the intensity at the rest frequency ν_l and τ_{ν_l} is the Sobolev optical depth of l th line, defined as $\tau_{\nu_l} = \kappa_l \rho \frac{c}{v_l} \left(\frac{dr}{dv}\right)$. The integration is performed over the complete visible disk of the star.

Following CAK, the line acceleration can be rewritten in terms of the force multiplier as a function of the optical depth parameter t . Where t is defined as:

$$t = \sigma_e^{\text{ref}} v_{\text{th}} \rho \frac{dr}{dv} \quad (21)$$

with v_{th} being the thermal velocity of the protons and σ_e^{ref} is some reference value for the electron scattering $\sigma_e^{\text{ref}} =$

$0.325 \text{ cm}^2 \text{ g}^{-1}$ (see *ISW*, Chapt. 8). The line acceleration in terms of the continuum acceleration is give by:

$$g_L = g_e M(t) \quad (22)$$

If the star is assumed to be a point source, $M(t)$ can be approximated by a simple power law parameterization (CAK, Abbott 1982):

$$M_{\text{point}}(t) = k t^{-\alpha} \left(\frac{n_e}{W} \right)^\delta \quad (23)$$

where the $(n_e/W)^\delta$ accounts for the effect of the electron density on the ionization balance in the wind. Here n_e is the electron density in units of 10^{11} cm^{-3} and W is the geometric dilution factor.

Friend & Abbott (1986) and Pauldrach et al. (1986) showed the importance of the finite disk correction on the line force in case of an extended source. This finite disk correction factor D_{fd} is given by (CAK):

$$D_{\text{fd}} = \frac{M(t)}{M_{\text{point}}(t)} = \frac{1}{N} \oint I(\theta, \phi) \left(\frac{(1+\sigma)}{1+\sigma\mu^2} \right)^\alpha \mu d\Omega \quad (24)$$

where

$$\sigma = \frac{r}{v} \frac{dv}{dr} - 1 \quad \text{and} \quad N = \frac{L_\star R_\star}{r} \quad (25)$$

This expression is completely general: the actual shape of the star and its intensity distribution enter through the integration domain and the $I(\theta, \phi)$ dependence. However, here we assume the intensity I to be locally isotropic, i.e. we neglect limb darkening. We have tested the effect of limbdarkening. The inclusion of limbdarkening results in a small θ -independent correction on D_{fd} .

The line acceleration g_L including all the necessary correction factors is now given by:

$$g_L = \left(\frac{\sigma_e}{4\pi} \right)^{1-\alpha} \frac{k L_\star}{r^2 c} (v_{\text{th}} F_m)^{-\alpha} D_{\text{fd}} \left(r^2 v \frac{dv}{dr} \right)^\alpha \left(\frac{n_e}{W} \right)^\delta \quad (26)$$

Combining Eqs. 17 and 26 gives the full equation of motion for the sectorial wind of a rotating star

$$0 = \left(1 - \frac{a^2}{v^2} \right) r^2 v \frac{dv}{dr} + GM_\star (1 - \Gamma_e) - 2a^2 r - v_{\text{rot}}^2 \frac{R_\star^2}{r} - \left(\frac{\sigma_e}{4\pi} \right)^{1-\alpha} \frac{k L_\star}{c} (v_{\text{th}} F_m)^{-\alpha} D_{\text{fd}} \left(\frac{n_e}{W} \right)^\delta \left(r^2 v \frac{dv}{dr} \right)^\alpha \quad (27)$$

4. Solutions of the equation of motion

For line driven winds of non-rotating stars solutions of the equation of motion have been retrieved by e.g. CAK and Pauldrach et al. (1986). These will be presented to serve as an illustration of the solution of the equation of motion and as a basis to interpret the more complicated results from the full equation of motion (27).

4.1. Simplified solutions for non-rotating star

4.1.1. The point source approximation

If the star is considered to be a point source the integral of the line acceleration in Eq. 20 collapses to one point. In this case D_{fd} disappears from Eq. 26 and the line acceleration becomes a simple function $g_L = \frac{C}{r^2} (r^2 v \frac{dv}{dr})^\alpha$. The solution of Eq. 17 was found by CAK and can easily be explained by neglecting the gas pressure terms (a^2). In this case Eq. 17 reduces to

$$r^2 v \frac{dv}{dr} = GM_\star (1 - \Gamma_e) + C \left(r^2 v \frac{dv}{dr} \right)^\alpha \quad (28)$$

where C is a constant containing the mass loss rate. The equation is solved by imposing uniqueness of the solution (Kudritzki et al. 1989) which then fixes the value of the constant and thus \dot{M} . The solution for the mass loss and velocity law is given by

$$\dot{M} = \frac{4\pi}{\sigma_e v_{\text{th}}} \left(\frac{\sigma_e}{4\pi} \right) \left(\frac{1-\alpha}{\alpha} \right)^{\frac{1-\alpha}{\alpha}} (k\alpha)^{\frac{1}{\alpha}} \left\{ \frac{n_e}{W} \right\}^{\frac{\delta}{\alpha}} \left(\frac{L_\star}{c} \right)^{\frac{1}{\alpha}} \{GM_\star (1 - \Gamma_e)\}^{\frac{\alpha-1}{\alpha}} \quad (29)$$

$$v(r) = v_\infty \left(1 - \frac{R_\star}{r} \right)^{0.5} \quad (30)$$

with

$$v_\infty = \sqrt{\frac{\alpha}{1-\alpha}} v_{\text{esc}} = \sqrt{\frac{\alpha}{(1-\alpha)}} \frac{2GM_\star (1 - \Gamma)}{R_\star} \quad (31)$$

This simplified solution is equal to the full CAK solution, in the limit of small sound speed, $a \ll v_{\text{esc}}$ (see also *ISW* Chapt 8).

4.1.2. Simple finite disk correction

In case of a homogeneous spherical star the finite disk correction factor D_{fd} (Eq. 24) can be calculated analytically (CAK):

$$D_{\text{fd}} = \frac{2}{(1 - \mu_\star)} \int_{\mu_\star}^1 \left(\frac{(1+\sigma)}{1+\sigma\mu^2} \right)^\alpha \mu d\mu = \frac{(1+\sigma)^{\alpha+1} - (1+\sigma\mu_\star^2)^{\alpha+1}}{(1 - \mu_\star^2)(\alpha+1)\sigma(1+\sigma)^\alpha} \quad (32)$$

Including the finite disk correction results in an increase in v_∞ , a decrease in \dot{M} and a modification of the simple scaling laws that were found in the original CAK approach (see Friend & Abbott 1986; Pauldrach et al. 1986). The decrease of the mass loss rate compared to the point source case is due to the decrease in g_L close to

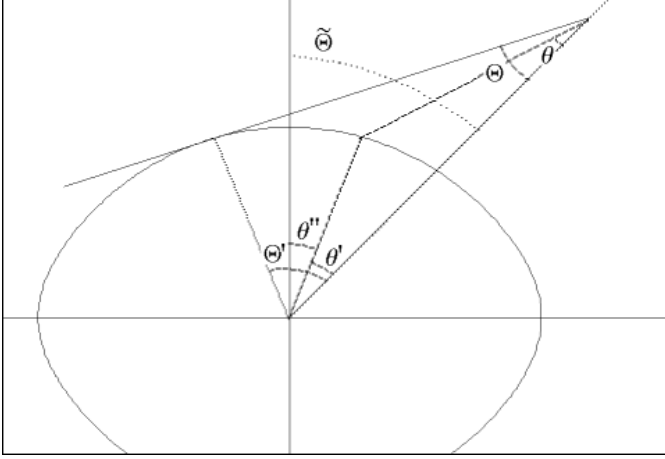


Fig. 2. Geometry for the calculation of the correction factors D_{fd} and D_c . A point on the ray with co-latitude $\tilde{\theta}$ sees a different limb angle Θ for every ϕ (not drawn; it is the angle around the line from stellar center to observer, not to be confused with the stellar longitude). The integrals in D_{fd} and D_c are over $0 < \phi < 2\pi$ and $0 < \theta < \Theta$. These are rewritten to integrals over the star centered angles θ' ($0 < \theta' < \Theta'$) and $\phi' = \phi$. The stellar radius and flux are given as a function of θ'' , the co-latitude, which can be calculated for every θ' and ϕ : $\theta'' = \theta''(\theta', \phi)$.

the star where \dot{M} is determined. Close to the stellar photosphere the finite disk correction is smaller than one, viz. $D_{fd}(r = R_*) = 1/(1 + \alpha) < 1$. The accompanying increase in v_∞ of typically a factor of two is due to two effects: (1) a reduction of \dot{M} results in a smaller amount of material to be accelerated and (2) far from the photosphere, the correction factor D_{fd} becomes larger than 1. The resulting dependence between v_∞ and v_{esc} is approximated by Friend & Abbott (1986):

$$v_\infty/v_{esc} \approx 2.2 \left(\frac{\alpha}{1 - \alpha} \right) \left(\frac{v_{esc}}{10^3 \text{ km/s}} \right)^{0.2} \quad (33)$$

They also found a relation for the modified mass loss rate:

$$\dot{M} \approx 0.5 \dot{M}_{CAK} \left(\frac{v_{esc}}{10^3 \text{ km/s}} \right)^{-0.3} \quad (34)$$

4.2. Solution of the equation of motion for the wind of a rotating star

The solution of Eq. 27 gives the mass loss rate, or rather the local mass loss rate $F_m(\theta)$, and velocity structure of the wind. The solution is complicated however by the presence of D_{fd} . This is an integral of a velocity-dependent function times the surface intensity over the visible section of the star. The appearance of the star varies throughout the wind in intensity distribution as well as in shape, as the star is no longer spherical and T_{eff} is a function of latitude. Since the analytic solution would be cumbersome, a

numerical approach of the solution is chosen. This is done with the analytic solutions of simple, i.e. the non-rotating, models in mind for comparison. The numerical solution of Eq. 27 is relatively straightforward in case the function D_{fd} is a given function of r . Therefore we solve Eq. 27 with $D_{fd}(r)$ in an iterative way as follows:

1. A β law for $v(r)$ is assumed, viz. $v(r) = (1 - R_*/r)^{0.5}$.
2. $D_{fd}(r)$ is calculated using this velocity law. Note that D_{fd} is not dependent on the actual value of $v(r)$ but on the velocity gradient.
3. Eq. 27 is solved using this correction factor $D_{fd}(r)$, obtaining a new velocity law $v(r)$.
4. Step 2-3 are repeated until convergence is reached.

Typically three iterations are sufficient, since further iterations changed the obtained values by less than 0.5 %. We checked that the solutions converged to the same value, independent of the starting value.

4.3. The calculation of $D_{fd}(r)$ and the continuum correction factor D_c

The calculation of the correction factor D_{fd} from the velocity law (step 1. in the scheme described above) is performed by numerical evaluation of Eq. 24. This is a non-trivial task, since both the integrand (Eq. 7) and the shape of the visible "disk" (Eq. 4) are dependent on r .

The main parameters needed to obtain D_{fd} for a fixed co-latitude $\tilde{\theta}$ are: the stellar surface $R(\theta)$ and the surface temperature $T(\theta)$, both given as a function of the co-latitude θ , as well as the velocity law $v(r)$. It is convenient to change the integration variables in Eq. 24 from the wind centered coordinates θ and ϕ to the star centered coordinates θ' and ϕ . For the definition of these coordinates, see Fig. 2. Note that here ϕ is not the stellar longitude anymore, but the angle of rotation around the line from a point (r, θ) in the wind to the stellar center.

$$\begin{aligned} D_{fd} &= \frac{1}{N} \int_0^{2\pi} \int_0^{\Theta(\phi)} I \left(\frac{(1 + \sigma)}{1 + \sigma \cos^2 \theta} \right)^\alpha \cos \theta \sin \theta \, d\theta d\phi \\ &= \frac{1}{N} \int_0^{2\pi} \int_0^{\Theta'(\phi)} I \left(\frac{(1 + \sigma)}{1 + \sigma \cos^2 \theta} \right)^\alpha \cos \theta \sin \theta \, \frac{d\theta}{d\theta'} d\phi \end{aligned} \quad (35)$$

where I is the frequency-integrated intensity

$$I = I(\theta', \phi) \propto T(\theta')^4 \quad (36)$$

The angles are related to one another via

$$\cos \theta = \frac{r - R(\theta', \phi) \cos \theta'}{\sqrt{(r - R(\theta', \phi) \cos \theta')^2 + (R(\theta', \phi) \sin \theta')^2}} \quad (37)$$

with the stellar surface given by $R(\theta', \phi) = R(\theta'')$, and

$$\cos \theta'' = \sin \theta' \cos \phi \sin \omega + \cos \theta' \cos \omega \quad (38)$$

Equation 35 can be integrated, considering that the limb angle $\Theta'(\phi)$ can be determined numerically, yielding the finite disk correction for the line acceleration of an arbitrary shaped star.

The correction factor D_c for the electron acceleration (defined in Eq. 16) similarly becomes:

$$D_c = \frac{1}{N} \int_0^{2\pi} \int_0^{\Theta'} I \cos \theta \sin \theta \frac{d\theta}{d\theta'} d\theta' d\phi \quad (39)$$

This correction is also included in the solution of the equation of motion.

4.4. Solving the equation of motion

To solve the equation of motion it is necessary to determine the conditions at the critical point: r_c , v_c and v'_c , or, equivalently, r_c , v_c and $v_0 = v(R_*)$, as well as the local mass loss rate F_m . Apart from Eqs. 18 and 19 and the equation of motion (27) itself the additional constraint for the continuum optical depth τ_e at the stellar radius is necessary (Pauldrach et al. 1986) to uniquely determine these quantities:

$$\tau_e(\theta) = \int_{R_*}^{\infty} \rho \sigma_e dr = \frac{2}{3} \quad (40)$$

If the condition for v_0 is used one may adopt any small value, say $v_0 = 0.1$ km/s, since even a large error in v_0 will only yield a relatively small error in v_∞ and F_m . This is due to the fact that at the surface of the star $v(r)$ and thus also ρ vary exponentially with scale height $H = \frac{a^2 R_*^2}{GM_{\text{eff}}} \ll R_*$. This means that the radius where Eq. 40 is fulfilled is very close to R_* . This has been checked a posteriori. In our calculations we have adopted this boundary condition for v_0 in the solution of the full momentum equation.

A first guess for the local mass loss rate obtained from the CAK solution is used to integrate the equation of motion from the stellar surface outward. This gives an approximate value for the critical point where $r^2 v \frac{dv}{dr} = 0$ if $F_m(\text{guess}) < F_m(\text{solution})$. This approximate value for the critical point can then be used to consecutively improve the guessed value of F_m using Eqs. 18 and 19. This iterative procedure is terminated when the local mass loss rate converges. The calculation is then completed by integrating past the critical point on the solution which extends to infinity (see CAK or Abbott 1980 for a description of the topology of the solutions). To deal with a numerical singularity at the sonic point the equations are solved for $r(v)$ rather than for $v(r)$.

5. Application to B[e] winds

5.1. A typical B[e] supergiant

We have calculated models for rotating B[e] stars using the above described method. For the first models we adopted

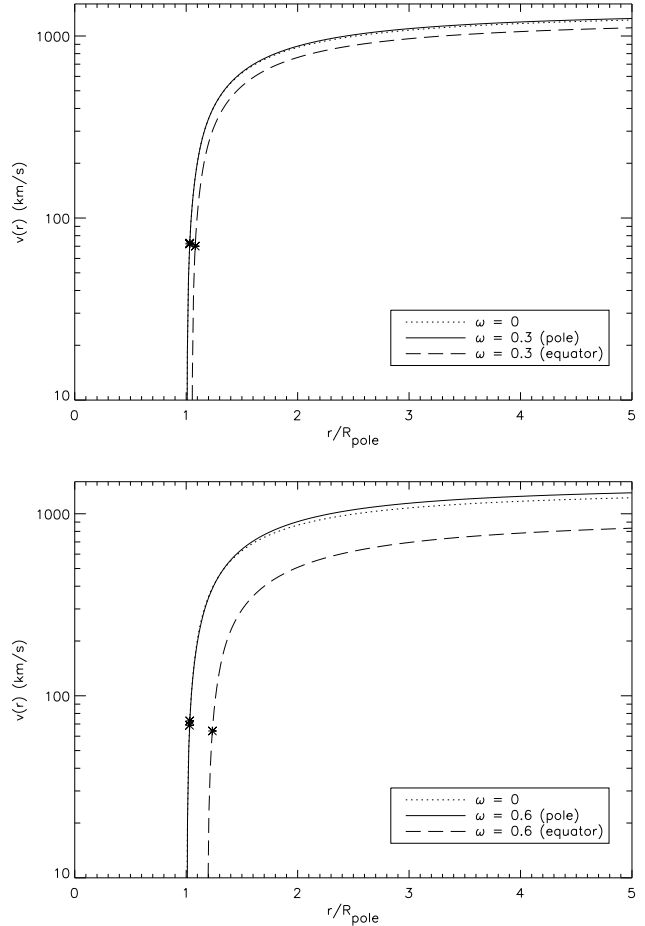


Fig. 3. The velocity law $v(r)$ at the pole and equator of B[e] wind models for different rotation rates. Top panel: $\omega = 0.3$, bottom panel: $\omega = 0.6$. The crosses indicate the location of the critical point of the wind. Note that the equatorial curves in the rotating models start at a radius $r/R_{\text{pole}} > 1$ due to the oblateness of the star (see text for stellar parameters).

the following stellar parameters, which are typical for B[e] stars: $L_* = 10^{5.5} L_\odot$, $M_* = 40 M_\odot$, $R_{*,\text{pole}} = 47 R_\odot$, $T_{\text{eff}} \simeq 20\,000$ and solar abundances. The effective temperature is defined as $T_{\text{eff}} = (L_*/\sigma_B S)^{0.25}$ where S is the total surface of the distorted star. The following force multiplier parameters from Pauldrach et al. (1986) were adopted to describe the line acceleration: $\alpha = 0.565$, $k = 0.32$, $\delta = 0.02$. An overview of the results for this generic B[e] star rotating at $\omega = 0, 0.3, 0.4, 0.5$ and 0.6 times the critical rotation speed is given in Table 1. The calculation of models with higher values of ω runs into numerical problems, because in the iteration, the approximate critical point can be below the sonic point. The table shows for different co-latitudes θ and different rotation velocities ω the values of v_∞ , the local mass loss rate $F_m(\theta)$ and the value of the velocity law parameter β , obtained by fitting

Table 1. Properties of a typical rotating B[e] star model ¹

ω	$\theta = 0$			$\theta = \pi/8$			$\theta = \pi/4$			$\theta = 3\pi/8$			$\theta = \pi/2$		
	v_∞ ²	F_m ³	β ⁴	v_∞	F_m	β	v_∞	F_m	β	v_∞	F_m	β	v_∞	F_m	β
0	1.40	2.35	0.63												
.3	1.43	2.67	0.63	1.40	2.64	0.63	1.35	2.53	0.63	1.30	2.42	0.63	1.29	2.36	0.64
.4	1.44	2.95	0.63	1.40	2.88	0.62	1.31	2.70	0.62	1.23	2.46	0.63	1.20	2.34	0.64
.5	1.46	3.33	0.63	1.40	3.23	0.62	1.27	2.95	0.62	1.14	2.53	0.64	1.11	2.27	0.66
.6	1.48	3.83	0.63	1.40	3.70	0.62	1.21	3.29	0.60	1.04	2.61	0.64	1.01	2.11	0.70

(1) The adopted stellar parameters are:

 $T_{\text{eff}} = 20000$ K, $L_\star = 10^{5.5} L_\odot$, $M_\star = 40 M_\odot$, $R_\star = 47 R_\odot$, $\alpha = 0.565$, $k = 0.32$, $\delta = 0.02$, solar abundances.(2): the terminal velocity v_∞ is in 10^3 km/s(3): the mass flux F_m in $10^{-6} M_\odot \text{y}^{-1}$ (4): the velocity law parameter β is obtained from a nonlinear fit of $v(r)$ from $1.1 R_\star$ to $10 R_\star$.**Table 2.** Properties of rotating B[e]¹ models: with different values of L_\star

L_\star L_\odot	ω	v_{inf}^{pole} 10^3 km s^{-1}	F_m^{pole} $10^{-8} M_\odot \text{y}^{-1}$	v_{inf}^{eq} 10^3 km s^{-1}	F_m^{eq} $10^{-8} M_\odot \text{y}^{-1}$	$\frac{\rho_{eq}}{\rho_{pole}}$	\dot{M} $10^{-8} M_\odot \text{y}^{-1}$
$10^{4.5}$	0	2.84	3.01			1	3.01
	0.3	2.91	3.37	2.60	3.04	1.01	3.18
	0.4	2.97	3.67	2.42	3.03	1.01	3.32
	0.5	3.04	4.08	2.22	2.98	1.00	3.50
	0.6	3.11	4.62	2.00	2.82	0.95	3.71
L_\star L_\odot	ω	v_{inf}^{pole} 10^3 km s^{-1}	F_m^{pole} $10^{-7} M_\odot \text{y}^{-1}$	v_{inf}^{eq} 10^3 km s^{-1}	F_m^{eq} $10^{-7} M_\odot \text{y}^{-1}$	$\frac{\rho_{eq}}{\rho_{pole}}$	\dot{M} $10^{-7} M_\odot \text{y}^{-1}$
$10^{5.0}$	0	2.06	2.53			1	2.53
	0.3	2.11	2.84	1.88	2.55	1.00	2.67
	0.4	2.15	3.11	1.75	2.54	1.00	2.79
	0.5	2.19	3.46	1.61	2.49	0.98	2.94
	0.6	2.24	3.93	1.46	2.35	0.91	3.15
L_\star L_\odot	ω	v_{inf}^{pole} 10^3 km s^{-1}	F_m^{pole} $10^{-6} M_\odot \text{y}^{-1}$	v_{inf}^{eq} 10^3 km s^{-1}	F_m^{eq} $10^{-6} M_\odot \text{y}^{-1}$	$\frac{\rho_{eq}}{\rho_{pole}}$	\dot{M} $10^{-6} M_\odot \text{y}^{-1}$
$10^{5.5}$	0	1.40	2.35			1	2.35
	0.3	1.43	2.67	1.29	2.36	0.98	2.47
	0.4	1.44	2.95	1.20	2.34	0.95	2.56
	0.5	1.46	3.33	1.11	2.27	0.90	2.71
	0.6	1.48	3.83	1.01	2.11	0.80	2.89
L_\star L_\odot	ω	v_{inf}^{pole} 10^3 km s^{-1}	F_m^{pole} $10^{-5} M_\odot \text{y}^{-1}$	v_{inf}^{eq} 10^3 km s^{-1}	F_m^{eq} $10^{-5} M_\odot \text{y}^{-1}$	$\frac{\rho_{eq}}{\rho_{pole}}$	\dot{M} $10^{-5} M_\odot \text{y}^{-1}$
$10^{6.0}$	0	0.65	3.93			1	3.93
	0.3	0.62	4.97	0.60	3.80	0.78	4.25
	0.4	0.59	6.00	0.58	3.61	0.62	4.54
	0.5	0.55	7.79	0.56	3.24	0.41	5.01
	0.6	0.49	11.1	0.56	2.64	0.21	5.76

(1): The adopted stellar parameters are: $M_\star = 40 M_\odot$; $R_\star = 47 R_\odot$; $T_{\text{eff}} = 20000$ K.

the calculated velocity structure from $1.1 R_\star$ to $10 R_\star$ to a β -law. We see that the value of β does not change much.

Fig. 3 shows the velocity structure of the wind and the location of the critical point for $\omega = 0, 0.3$ and 0.6 . Note that the critical point is very close the star. This is true for all finite disk corrected solutions. Figure 4 shows the behaviour of v_∞ versus F_m for various rotational speeds and latitudes. As expected, v_∞ at the equator is smaller

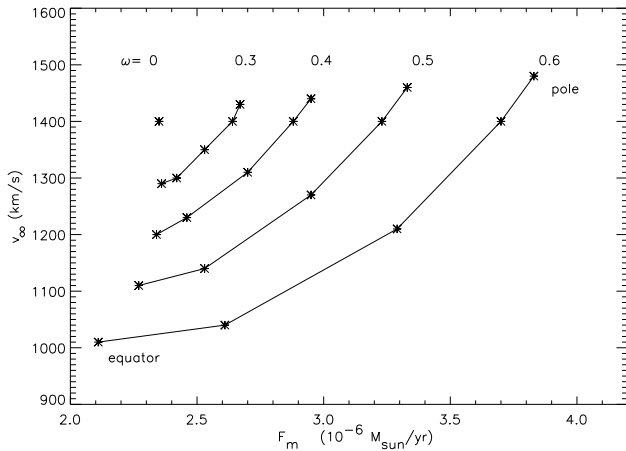
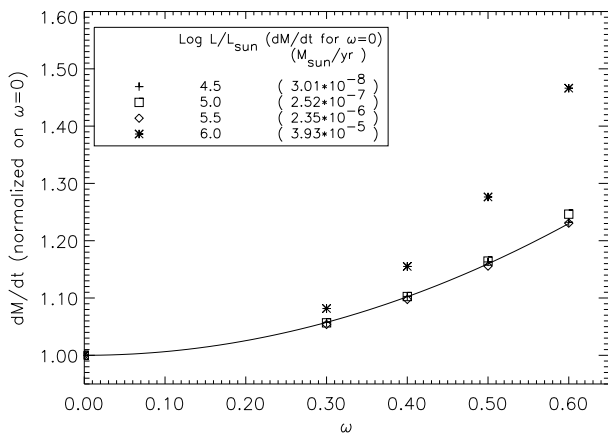
than at the pole because v_∞ scales roughly with v_{esc} and due to the smaller value of v_{esc} at the equator.

Figure 5 shows the latitude dependence of the local mass-loss rate and of the terminal velocity from equator to pole, for different rotational speeds, indicated by ω . At the pole ($\theta = 0$) v_∞ is about constant for various rotational speeds. The mass-loss rate at the equator decreases slightly with increasing rotation. The increase of

Table 3. Properties of rotating B[e] ¹ models: with different values of M_*

M_* M_\odot	ω	v_{inf}^{pole} 10^3 km s^{-1}	F_m^{pole} $10^{-6} M_\odot \text{ yr}^{-1}$	v_{inf}^{eq} 10^3 km s^{-1}	F_m^{eq} $10^{-6} M_\odot \text{ yr}^{-1}$	$\frac{\rho_{eq}}{\rho_{pole}}$	\dot{M} $10^{-6} M_\odot \text{ yr}^{-1}$
20	0	0.80	5.66			1	5.66
	0.3	0.80	6.64	0.73	5.67	0.94	5.69
	0.4	0.80	7.49	0.68	5.58	0.88	6.00
	0.5	0.79	8.74	0.64	5.32	0.75	6.38
	0.6	0.79	10.5	0.60	4.76	0.53	6.81
60	0	1.82	1.55			1	1.55
	0.3	1.85	1.76	1.66	1.56	0.99	1.55
	0.4	1.89	1.92	1.56	1.55	0.98	1.59
	0.5	1.91	2.16	1.43	1.51	0.93	1.68
	0.6	1.95	2.46	1.31	1.41	0.85	1.75

(1): The adopted stellar parameters are: $L_* = 10^{5.5} L_\odot$; $R_* = 47 R_\odot$; $T_{\text{eff}} = 20000 \text{ K}$.

**Fig. 4.** The latitude dependence of the mass-loss rate and v_∞ of a typical B[e] star, for various rotational speeds. (See text for stellar parameters).**Fig. 5.** Mass loss rates for different rotation speeds. The drawn line is given by: $1 + 0.64\omega^2$

the mass loss rate at the equator as calculated by Pauldrach et al. (1986) and Friend & Abbott (1986) is offset by a decrease in mass loss rate due to the smaller radiative flux at the equator due to the von Zeipel effect. The mass loss rate at the pole increases strongly with increasing rotation rate due to the increase in luminosity at the pole. This is because the total luminosity of the star is fixed and the smaller luminosity at the equator must therefore be compensated by a higher luminosity at the pole.

5.2. The overall density properties

The overall effect of rotation is to increase the mass loss rate of a star. This can be seen in Fig. 5 where the overall mass-loss rate (i.e. F_m integrated over the stellar surface) is plotted vs. the rotational velocity. The mass-loss rate of the models with $4.5 \leq \log L_*/L_\odot \leq 5.5$ vary with ω as $1 + 0.64\omega^2$.

Figure 6 shows the resulting density contrast (far from the star) between pole and equator ($\rho_{eq}/\rho_{pole} = F_m^{eq} v_\infty^{pole} / F_m^{pole} v_\infty^{eq}$). The densities at pole and equator are essentially the same: the smaller v_∞ at the equator is offset by the larger mass loss rate F_m at the pole.

5.3. Varying L_*

We have also calculated models for different luminosities (see Table 2), and different stellar masses (see Table 3). The mass-loss rate for the different luminosities is also plotted in Fig. 5. The density contrast for various luminosities is plotted in Fig. 6. We see that the density at the pole compared to the equator increases for increasing luminosity and the effect on the mass-loss rate is only visible for the highest luminosity. This is an effect of the continuum acceleration D_c . Fig. 7 illustrates the effect of the continuum acceleration on the forces in the wind for a star with high luminosity ($\Gamma_e = 0.76$). The net effect

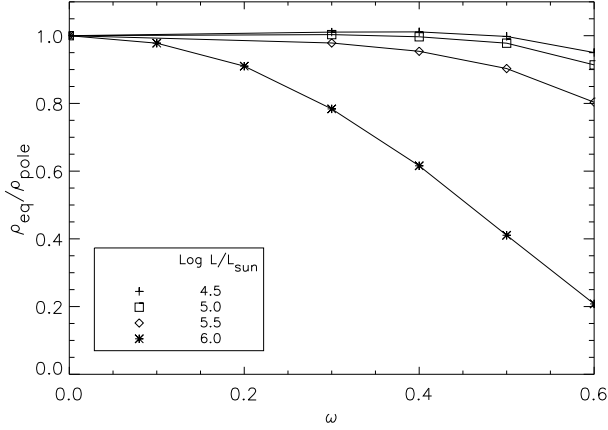


Fig. 6. The density contrast $\rho^{\text{eq}}/\rho^{\text{pole}}$ for various values of $\log L_*/L_\odot$.

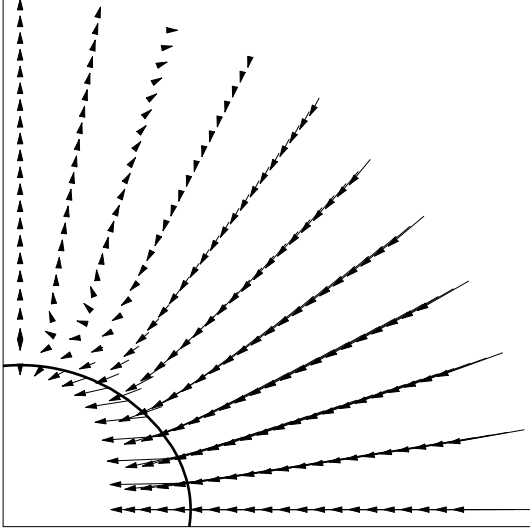


Fig. 7. Vector plot of the gravity (F_g) and the continuum radiation force (F_e). The vectors indicate strength and direction of $r^2(F_g + F_e)$ on an arbitrary scale for a star with $\Gamma_e = 0.76$ and $\omega = 0.6$. Note that line forces and centrifugal forces are not included.

of the continuum radiation pressure and the gravity, i.e. $GM_*(1 - \Gamma'_e)/r^2$, is an inward force in the equatorial region and an outward force in the polar region where the flux is higher.

For small luminosity the variation in Γ'_e through D_c is not important because Γ_e itself is small. For high luminosity $L_*/(GM_*)$ increases and thus the effect of D_c on Γ'_e becomes noticeable (this is with all other properties of the star fixed). In Eq. 31 we see that a larger value of D_c at the pole causes a relatively larger decrease (through Γ'_e) in v_{esc} and thus in v_∞ , whereas the mass loss rate at the equator will increase less because of the smaller D_c . This is only a qualitative explanation and the actual depen-

dence of $\rho_{\text{eq}}/\rho_{\text{pole}}$ does not follow the relation suggested by Eqs. 29 and 31. We have found that the actual values of $\rho_{\text{eq}}/\rho_{\text{pole}}$ could be approximated quite well (within 10 percent) with the following relation:

$$\rho_{\text{eq}}/\rho_{\text{pole}} \approx \left\{ \frac{1 - \Gamma'_e(\theta = 0, r/R_{\text{eq}} = 1)}{1 - \Gamma'_e(\theta = \pi/2, r/R_{\text{eq}} = r_{\text{min}})} \right\}^{1.5} \quad (41)$$

where the $r_{\text{min}} \approx 1.2$ is the radius where D_c reaches its minimum value.

So we see that although rotation alone modifies the wind structure considerably, it cannot be responsible for the density contrast between the equatorial and polar wind observed in B[e] stars, in case only radial effects are considered. We conclude that at least one other physical effect must be responsible for the formation of disks of rotating B[e] stars. The two most likely additional effects are the bi-stability and the flow of the wind material towards the equator.

6. Rotationally induced bi-stability models

In the section above we have shown that rotation alone cannot explain the observed large density contrast between the poles and the equator of B[e] stars. One of the possible additional mechanisms to enhance this contrast is the bi-stability jump.

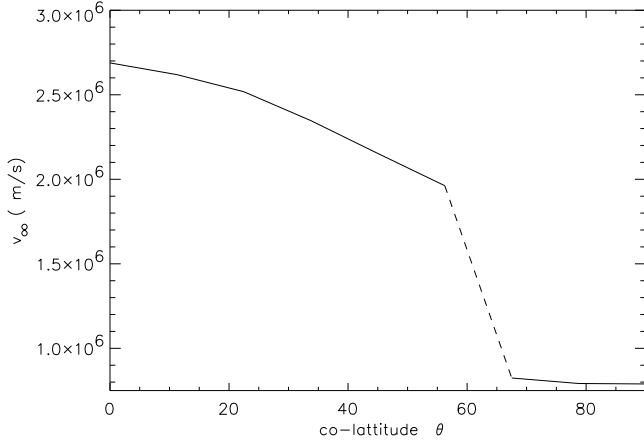
To investigate whether the bi-stability jump observed in normal B-supergiants can explain the formation of disks around B[e] stars, we have calculated bi-stable wind models for a fast rotating typical B[e] supergiant. Spherical, NLTE wind models for normal B supergiants have been calculated by Vink et al. (1999). From these models CAK-like force multiplier parameters have been derived using a Monte-Carlo method to simulate photon-gas interactions. These models show the occurrence of a bi-stability jump around $T_{\text{eff}} \simeq 25000$ K.

For two models on either side of the bi-stability jump ($T_{\text{eff}} = 17\,500$ and $30\,000$ K), the CAK parameters were determined by fitting a power law from about the sonic point to about $0.5v_\infty$ (from $t = 10^{-2}$ to $t = 10^{-4}$ in optical depth, t is defined in Eq. 21) to the calculated force multiplier values. The resulting values for k , α and δ are listed in Table 4. Note that the δ parameter is taken equal to zero as it was not possible to extract it explicitly from the models. Its effect is hidden in the constant k . As expected, the values for the force multiplier parameters are quite different for the two cases, because the ionization has changed dramatically over the bi-stability jump.

The predicted bi-stability jump occurs around $T_{\text{eff}} \simeq 25$ kK. Therefore we calculated a model for a rotating B[e] star with the following properties: $T_{\text{eff}} = 25000$ K, $L_* = 10^5 L_\odot$, $M_* = 17.5 M_\odot$ and solar abundances. This implies that the pole of the rapidly rotating star will be hotter than 25 kK and the equator will be cooler than 25 kK.

Table 4. The force multiplier parameters for a bi-stable wind

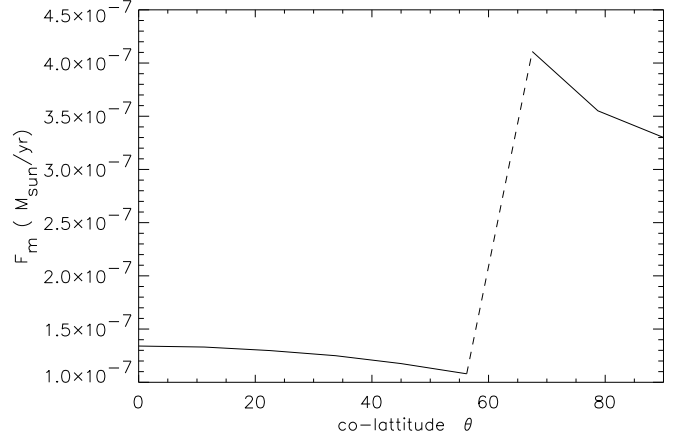
T_{eff}	k	α	δ
17500 K	0.57	0.45	0.0
30000 K	0.06	0.65	0.0

**Fig. 8.** The terminal velocity v_{∞} for a star with a bi-stability jump as a function of co-latitude. The dashed part indicates the location of the bi-stability jump. Notice the drastic drop by about a factor 3 around $\theta=60^\circ$, due to the bi-stability jump. (See text for the adopted stellar parameters)

For the pole, the force multipliers k and α from the hot Monte Carlo model of 30 000 K were used, whereas for the equator, k and α from the cool model of 17 500 K were used.

The resulting $v_{\infty}(\theta)$ and mass loss rates $F_m(\theta)$ are plotted in Figs. 8 and 9 for $\omega = 0.6$. Clearly visible is the drastic decrease in v_{∞} and the drastic increase of F_m towards the equator. This occurs around a co-latitude θ (angle from the pole) of about 60 degrees, where $T_{\text{eff}} \simeq 25\,000$ K. (The precise location of the jump depends on the effective temperature of the star). Since both F_m and v_{∞} have a equator/pole contrast of about a factor of three, the resulting density contrast is about a factor of 10 in a disklike region with a half opening angle of 30 degrees.

Our calculations show that the density contrast in the wind between pole and equator due to the bi-stability jump is significantly larger than without the bi-stability jump. Yet, the calculated value of about a factor 10 is not sufficient to explain the observed density contrast of a factor ~ 100 . So another mechanism is needed to enhance the density contrast even further. This is most likely the wind compression mechanism (Bjorkman & Cassinelli 1993; Bjorkman 1998).

**Fig. 9.** The mass loss rate F_m of a star with a bi-stability jump as a function of co-latitude. The dashed part indicates the location of the bi-stability jump. Notice the steep jump in mass loss rate near $\theta = 60^\circ$. (See text for the adopted stellar parameters)

7. Summary and discussion

We have modified the line driven wind theory for rotating stars by including the effects of oblateness and gravity darkening as well as rotational terms in the equation of motion. We considered a sectorial wind, i.e. we neglected the effect of the motion of the wind towards the equator or towards the pole. This assumption is justified close to the stellar surface below the critical point of the momentum equation. This implies that our method will predict about the correct distribution of mass-loss rates from the star as a function of stellar latitude, but it may not be accurate enough to predict the velocity and density distribution further away from the star, if motions in the θ direction become important.

The equation of motion was solved using an iterative numerical scheme, that includes the conservation of angular momentum and the correction factors to the radiative acceleration by lines and by the continuum, due to the non-spherical shape of the star and due to the latitude dependence of the radiative flux. This method was applied to study its possible effects on the formation of disks around fast rotating B[e] supergiants.

The models with constant force multiplier parameters k , α and δ show a decrease of *both* the mass loss rate and the terminal velocity from pole to equator. This is mainly due to two effects: the reduction of the escape velocity from pole to equator, resulting in a higher terminal velocity at the pole, and the reduction of the radiative flux from the pole to the equator due to gravity darkening, which results in a decrease in mass loss rate at the equator.

For a star with a fixed luminosity and a fixed polar radius, the temperature at the pole increases and the temperature at the equator decreases with increasing rotation

rate. The terminal velocity of the wind from the poles is almost independent of v_{rot} but at the equator v_{∞} decreases with increasing rotation rate. The mass-loss rate at the pole increases with increasing v_{rot} , due to the increase in T_{eff} at the poles, but the mass loss rate from the equator is almost independent of the rotation. The combination of these effects alone produce a density contrast between the polar and the equatorial wind of a factor $\rho_{\text{eq}}/\rho_{\text{pole}} \simeq 1$, except for fast rotating stars with high luminosity (in which case $\rho_{\text{eq}}/\rho_{\text{pole}} < 1$).

Our results agree quantitatively with those obtained by Maeder (1999) for the latitudinal dependence of F_m . Our predictions of the global mass loss rates are also in general agreement with those of Maeder for models with luminosities far from the Eddington limit. For high luminosities we find a strong polar outflow, whereas Maeder's models predict an enhanced equatorial outflow on the basis of the original CAK scaling laws. This difference is due to the fact that we have included an improved description of the radiation pressure in a rotating star.

The difference between the polar wind and the equatorial wind is strongly enhanced when the bi-stability of radiation driven winds between $T_{\text{eff}} \simeq 20\,000$ and $30\,000$ K is taken into account. In this case the force multipliers k and α of a rapidly rotating star change drastically with stellar latitude if the pole is hotter than $25\,000$ K and the equator is cooler. In § 6 we have applied the newly calculated force multipliers from Vink et al. (1999) above and below the bi-stability jump to the models of rotating B[e] supergiants. One might argue that it is not allowed to apply the force multipliers of (bi-stable) spherical wind models to aspherical winds of rotating stars. However, we have shown that a disk formed through bi-stability will be sufficiently thick (typically about 30 degrees for a star with an effective temperature equal to about $25\,000$ K) to make these spherical models reasonable approximations for the conditions in the wind close to the star, where the mass loss rate is determined. We find that rotationally induced bi-stability models of B[e] stars reach a density contrast of about a factor 10 between the dense equatorial wind and the less dense polar wind. This is less than the factor 10^2 that is observed (see e.g. Bjorkman 1998).

The extra density increase is most likely due to the wind compression. The gas that leaves the photosphere from a rotating wind, will follow an orbit in a tilted plane defined by the local rotation vector and the center of the star. If the rotational velocity is large or the wind velocity is small, this orbit will cross the equatorial plane where the streamlines of the wind from different stellar latitudes cross. The resulting shock will compress the gas into a thin outflowing disk with an opening angle of only a few degrees (Bjorkman & Cassinelli 1993; *ISW* Chapt 11). We have not considered this wind compression in our model. However, it is likely to occur in rotationally induced bi-stable winds, because the wind velocity in the equatorial

plane is about a factor three smaller than from the poles, thus facilitating the wind compression.

Owocki & Cranmer (1994) have argued that the flow of the wind towards the equatorial plane, predicted in the WCD-theory, may be offset by a θ -component of the line acceleration towards the polar regions. This “disk inhibition” mechanism operates in wind models with constant force multipliers k and α . However, it is not clear that this mechanism is sufficiently strong to overcome the wind compression in the RIB-model. This is because k and α change with latitude in the RIB-model and there is a strong density gradient in the wind from the equator to the poles (Owocki et al. 1998, Puls et al. 1999).

The combination of the RIB and the WCD mechanism may offer the best possibility for explaining the disks of B[e]-supergiants. Whether the compression is strong enough to explain the observed high density contrast between the polar and the equatorial wind, remains to be seen. It can be calculated by combining the solutions of the wind momentum equation of rotating oblate stars with gravity darkening (derived in this paper), and the calculation of the resulting trajectories of the wind. The combination of the rotation induced bi-stability model and the wind compressed disk model is promising for explaining the disks of B[e] stars because the RIB-mechanism explains the increased mass loss and the small velocity from the equatorial regions and the WCD-mechanism explains the strong compression of the disk.

References

- Abbott D.C., 1980, ApJ 242, 1183
- Abbott D.C., 1982, ApJ 259, 282
- Bjorkman J.E., 1998, in *B[e] stars*, eds A.M. Hubert, C. Jaschek Kluwer: Dordrecht, ASSL 233, p 189
- Bjorkman J.E., Cassinelli J.P., 1993, ApJ 409, 429
- Cassinelli 1998 in *B[e] stars*, eds A.M. Hubert, C. Jaschek Kluwer: Dordrecht, ASSL 233, p 177
- Castor J.I., 1974, MNRAS 169, 279
- Castor J.I., Abbott D.C., Klein R.L., 1975, ApJ 195, 157
- Cranmer S.R., Owocki S.P., 1994, ApJ 440, 308
- Feldmeier A., 1999 in *Variable and non-spherical stellar winds in luminous hot stars*, Lecture Notes in Physics, eds. B. Wolf et al. Springer: Heidelberg, p 285.
- Friend D.B., Abbott D.C., 1986, ApJ 311, 701
- Gayley K.G., 1995, ApJ 454, 410
- Kudritzki R.P., Pauldrach A., Puls J., Abbott D.C., 1989, A&A 219, 205
- Lamers H.J.G.L.M., Cassinelli J.P., 1999, Introduction to Stellar Winds, Cambridge Univ. Press. (*ISW*)
- Lamers H.J.G.L.M., Pauldrach A., 1991, A&A 244, L5
- Lamers H.J.G.L.M., Snow T.P., Lindholm D.M., 1995, ApJ 455, 269
- Lamers H.J.G.L.M., Zickgraf F.-J., de Winter D., Houziaux L., Zorec J., 1998, A&A 340, 117
- Lucy L.B., 1982, ApJ 255, 286
- Maeder A., 1999, A&A 347, 185
- Owocki S.P., Castor J.I., Rybicki G.B., 1988, ApJ 335, 914
- Owocki S.P., Cranmer R.C., 1994, ApJ 424, 887

- Owocki S.P., Cranmer R.C., Gayley K.G., 1998, Ap&SS 260, 149
- Pauldrach A., Puls J., Kudritzki R.P., 1986, A&A 164, 86
- Puls J., Petrenz P., Owocki S.P., 1999 in *Variable and non-spherical stellar winds in luminous hot stars*, Lecture Notes in Physics, eds. B. Wolf et al. Springer: Heidelberg, p 131.
- Vink J.S., de Koter A., Lamers H.J.G.L.M., 1999, A&A 350, 181
- von Zeipel H., 1924, MNRAS 84, 665
- Zickgraf F.-J., 1992, in *Astronomical CCD Observing and Reduction Techniques*, ed. Howell S.B., ASP Conference Series Vol. 22, 75
- Zickgraf F.-J., Schulte-Ladbeck R.E., 1989, A&A 214, 274
- Zickgraf F.-J., Wolf B., Stahl O., Leitherer C., Klare G., 1985, A&A 143, 421